Melting Curve and High-Pressure Chemistry of Formic Acid to 8 GPa and 600 K

W. Montgomery,*,† J. M. Zaug,‡ W. M. Howard,‡ A. F. Goncharov,‡ J. C. Crowhurst,‡ and R. Jeanloz†

Department of Earth and Planetary Science, University of California, Berkeley, 307 McCone Hall, Berkeley, California 94720-4767, and University of California at Lawrence Livermore National Laboratory, Chemistry & Material Science Directorate, 7000 East Avenue, Livermore, California 94551

Received: April 15, 2005; In Final Form: August 12, 2005

We have determined the melting temperature of formic acid (HCOOH) as a function of pressure to 8.5 GPa using infrared absorption spectroscopy, Raman spectroscopy and visual observation of samples in a resistively heated diamond-anvil cell. The experimentally determined incongruent melting curve compares favorably with a two-phase thermodynamic model. Decomposition reactions were observed above the melting temperature up to a pressure of 6.5 GPa, with principal products being CO_2, H_2O, and CO. At pressures above 6.5 GPa, decomposition led to reaction products that could be quenched as solids to zero pressure, and infrared and Raman spectra indicate that pressure leads to the presence of sp3 carbon−carbon bonding in these reaction products.

Introduction

As the simplest carboxyl molecule, formic acid (O═CH−OH) offers an archetype for characterizing the effects of pressure on the hydrogen bonding, polymerization, and chemical kinetics of organic compounds. It is also of interest for understanding the origination of life because it is among the simplest "prebiotic" molecules present in space and has been observed in spectra from the interstellar medium, from around protostars and comets, and in meteorites (i.e., remnants of the building blocks of planets).[1−7] Pressure is relevant here because life can potentially be established more readily at depth, within a planetary body, than on the planetary surface where the prebiotic molecules are subject to the destructive effects of high-velocity impact from extraplanetary bolides and of ionizing radiation from space (unless a sufficiently dense atmosphere is present). Formic acid is also considered an important reaction intermediate in "maturation", that is, heating under pressure, of organic matter beneath the Earth's surface.[8]

Unlike other carboxylic acids, HCOOH does not form dimers in the liquid and solid states.[9] It instead forms an infinite network of hydrogen-bonded chains, which are linked by a hydroxyl group displaying a characteristic infrared-absorption band at ∼2600 cm^{-1} (Figure 1). Crystallization at ambient temperature and low pressure (<1 GPa) evidently involves forming links between the chains, as indicated by a shift of the O−H vibration frequency from ∼3000 to ∼2600 cm^{-1}.

A phase transition was reported previously to occur at 4.5 GPa and 300 K,[9] and a subsequent single-crystal diffraction study proposed a high-pressure crystal structure consisting of a more complex structure combining cis and trans isomers of HCOOH in symmetrically flat layers.[10] Recent powder X-ray diffraction data indicate that the low-pressure phase is stable to well over 30 GPa at 300 K, however, and we consequently do not consider solid−solid phase transformations in the present study.[11] Although ref 11 does not report any chemical reactions, its authors do observe the strengthening of the hydrogen bond between the hydroxyl hydrogen and carbonyl oxygen of neighboring molecules at pressures up to 12 GPa. This shift in bond strength at increased pressures foreshadows the decomposition reactions observed in the present study.

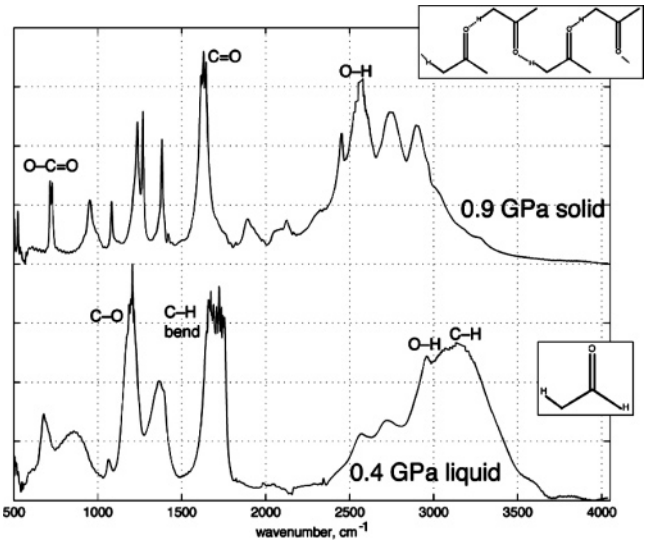

Figure 1. Comparison of infrared absorption spectra of single-crystal (top) and liquid (bottom) formic acid obtained at 298 K and at 0.9 and 0.4 GPa, respectively. Band assignments follow ref 9 and insets illustrate molecular structures.

Experimental Methods

Pure formic acid was obtained starting from 98% HCOOH, to which pthalic anhydride was added, and the mixture was refluxed (6 h under a dry atmosphere) and twice distilled (97−99 °C and 99−100 °C). Aliquots were then loaded into a membrane-type diamond-anvil cell containing type-II diamonds with 500-μm culets.[12] A pure Ir gasket with an initial thickness of ∼30 μm and a 220-μm diameter sample chamber was used

* Corresponding author. E-mail: wren@eps.berkeley.edu.
† University of California, Berkeley.
‡ University of California at Lawrence Livermore National Laboratory.

10.1021/jp051967y CCC: $30.25
Published on Web 09/23/2005

to contain each sample. Samples were heated at rates of less than 0.05 K/min to more than 1 K/min using a Eurotherm 2408 electronic temperature-control system powering an external heating ring that surrounds the diamond cell.

We made spectroscopic measurements during both the heating and cooling cycles. Changes in the infrared-absorption spectrum, as illustrated in Figure 1, combined with visual observation of liquification and crystallization, allowed us to determine the melting curve of formic acid as a function of pressure. Fourier transform infrared (FTIR) absorption and Raman spectra were obtained through a long working-distance microscope designed to accommodate heated diamond cells. Our FTIR system consists of a Bruker Optics Vector-33 interferometer and a glowbar source, in conjunction with liquid-nitrogen-cooled InSb and HgCdTe detectors, for complete coverage of the spectral ranges of interest at a resolution of 4 cm^{-1}. Raman and fluorescence signals are brought into a 0.8-m focal-length spectrometer by fiber optics and dispersed onto a thermoelectrically cooled CCD multichannel array by means of an 1800 lines/mm grating.

We monitored the pressure during heating and cooling using the fluorescence lines of $SrB_4O_7:Sm^{2+}$ (λ_{0-0})[13] and/or ruby ($Al_2O_3:Cr^{3+}$).[14] Optimally, both pressure sensors were included, but some experiments only used one sensor because of the loss of the second during loading. Temperature is monitored using type-K thermocouples from Omega Engineering secured against the gasket and one of the diamond anvils with gold foil. The temperature precision is ±0.5 K, but the absolute accuracy decreases with increasing temperature because of the high thermal conductivity of diamond, and was estimated to be +0 K and −4 K up to 575 K. The sample pressure was maintained to within 0.2 GPa throughout each experiment by monitoring the pressure gauge and adjusting the DAC membrane pressure accordingly.

Results

A. Solid−Liquid Transformation. Figure 2 shows the spectra acquired at a fixed pressure of 3.0 GPa and a constant heating rate of 1 K/min from 300 to 623 K. At 423 K, the hydroxyl peak at 3000 cm^{-1} shifts in position and intensity to a broad band at ~3500 cm^{-1}, indicating the formation of liquid HCOOH; this was confirmed by visual inspection (cf. Figure 1). Accompanying this phase transformation is a chemical reaction, the formation of CO_2, which is discussed in greater detail below. The melting curve presented is therefore an incongruent melting curve, with a chemical reaction accompanying the fusion process. Although only a small amount of CO_2 is formed, we distinguish between the spectroscopically determined appearance of CO_2 and the spectroscopic and visual appearance of liquid formic acid in the phase diagram.

Melting temperatures were obtained, through the combination of spectroscopic measurements and visual observation, over a range of pressure up to 8 GPa. To determine the equilibrium fusion curve, and overcome possible kinetic barriers, we characterized samples on both heating (melting) and cooling (crystallization) at different rates. Figure 3 illustrates such an experiment, with the sample heated and then cooled (not shown) at the slower rate of 0.05 K/min while at 3.4 GPa. A similar evolution is documented by the spectra, and the fact that melting occurs at a lower temperature than for the 1 K/min heating rate (as also confirmed by visual observation) implies that data collected at the faster heating rate provides only an upper bound on the melting curve because of kinetic hindrances (i.e., superheating).

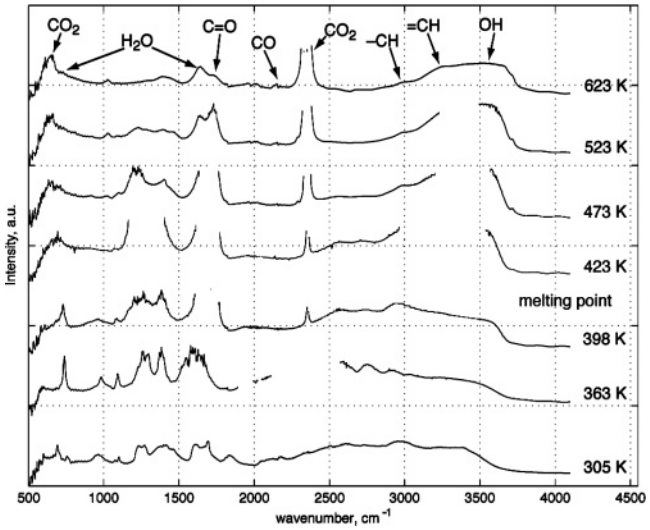

Figure 2. Temperature evolution of FTIR spectra of pure formic acid during isobaric heating and cooling at 3.0 GPa at a heating rate of 1 K/min (bottom to top). Each spectrum is collected in 127 s, and the complete heating−cooling cycle requires 6−12 h. The entire sample appears liquid at ~423 K, with the formation of a broad O−H peak at ~3450 cm^{-1} and the disappearance of the O−C−O torsional band at 680 cm^{-1}. CO_2 formation (strong band at 2350 cm^{-1}) is observed at 398 K, concurrent with the visual appearance of liquid droplets, which grow in size until the entire sample is liquid. Above 500 K, a δ-CO doublet is visible at 2130 and 2148 cm^{-1}. The formation of H_2O is determined by the appearance of secondary H_2O bands at 1620 cm^{-1} and a shoulder at ~600 cm^{-1}. Gaps in the spectra indicate regions of total absorption by the combined sample and anvils.

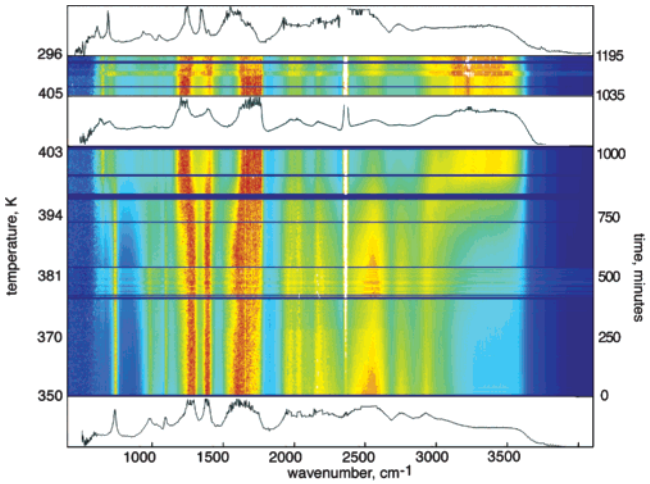

Figure 3. Temperature evolution of FTIR absorption spectra of pure formic acid during isobaric heating (0.05 K/min) and cooling at 3.4 GPa (bottom to top). Each spectrum is collected in 127 s, and the complete cycle of heating and cooling required more than 12 h. Spectra are shown at 350 and 403 K and then at 296 K on cooling, with colors indicating the time evolution in between (red for high absorption, blue for low absorption). In this case, formation of (solid) CO_2 is apparent at 360 K (white saturated band), whereas the sample appears solid both visually and spectroscopically up to 400 K. Only a small amount of carbon dioxide is formed (~5% estimated from band intensities at 400 K), and we find no Raman-spectroscopic evidence for the presence of molecular hydrogen, probably because of the increasing thermal background and the limitations of our spectrometer.

The present experimental constraints on the melting curve of formic acid are summarized in Figure 4. Both undercooling and superheating are reduced significantly by decreasing the rate at which temperature is changed, with the data suggesting

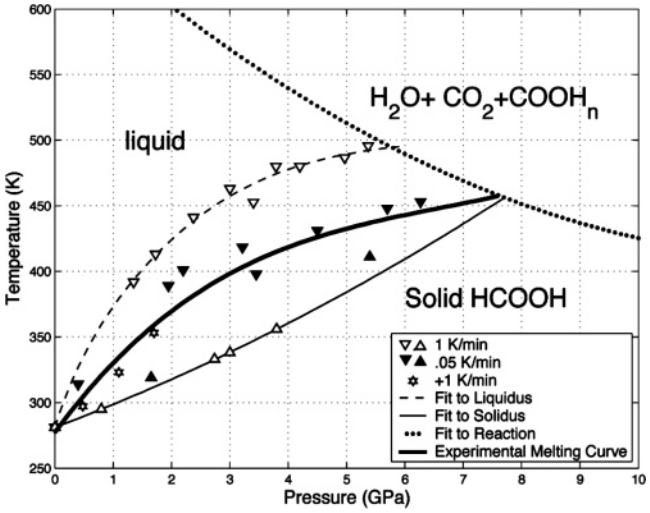

Figure 4. Solid triangles indicate upper bounds (downward pointing) and lower bounds (upward pointing) of the liquid−solid phase transition determined by slow heating/cooling rates of 0.05 K/min. Open triangles represent boundaries determined by rapid heating/cooling (1 K/min). The experimental melting curve (solid line) represents the average of experimental results upon slow heating and cooling.

that the fusion temperature is bracketed to better than ±20−30 K up to 8 GPa.

B. High-Temperature Decomposition of Formic Acid. The formation of simple hydrocarbons (C_2H_2, C_2H_4, and CH_4) from the thermal decomposition of formic acid has been established by Muller and Petryal[15] at room pressure and high temperature (1696 K). At high pressures, we have also observed irreversible reactions on heating liquid or solid HCOOH, and the products can be quenched to ambient conditions (Figure 5).

The spectra indicate that the molecular structure and bonding of the high-temperature reaction products vary with synthesis pressure. The lower-pressure sample clearly contains microcrystalline graphite, based on the Raman spectrum: D, G, and D′ bands are present.[20] The infrared-absorption spectrum indicates that other bonds, notably O−O and C−O−C, are present in some concentration. The higher-pressure solid product

TABLE 1: Assignment of the FTIR and Raman Bands Observed in the Spectrum of the Recovered Samples[a]

frequencies, cm^{-1}	assignment
870	O−O
1030	C−O−C
1100	
1190	
1260	C−C
1349.3	D-band microcrystalline graphite
1390	
1450	
1519.7	G-band microcrystalline graphite
1577	combined G- and D′- band nanocrystalline diamond
1580	C═C
1591.7	D′-band microcrystalline graphite
1740	C═O
2590	−C−H
2980	═C−H
∼3400	O−H

[a] Assigments have been made based on refs 20, 21, and 30.

is less easily characterized. The Raman spectrum shows a broad band at 1575 cm^{-1}, typical of disordered nanocrystalline diamond,[21] which has a high concentration of sp2 bonds, indicated by the presence of G and possibly D′ bands. The IR spectra confirm the disorder of this sample because only a few peaks are present in the higher-pressure sample. These spectra, combined with visual observations, suggest that compression and heating of HCOOH results in the production of macromolecules containing C, H, and O as well as the easily detected CO_2.

It is interesting that the spectra of the recovered solidlike products rule out the presence of formaldehyde, HCO free radicals, formate species (HCOO), furan, butadiene, or acetylene. Specifically, our spectra lack the sharp peaks at frequencies above 2900 cm^{-1} associated with formaldehyde and butadiene, the lower-frequency peaks associated with ring structures (furan), and the C≡C band and doublets of acetylene. None of our peaks overlap with the reported vibrational bands for formyl radicals or formate species.

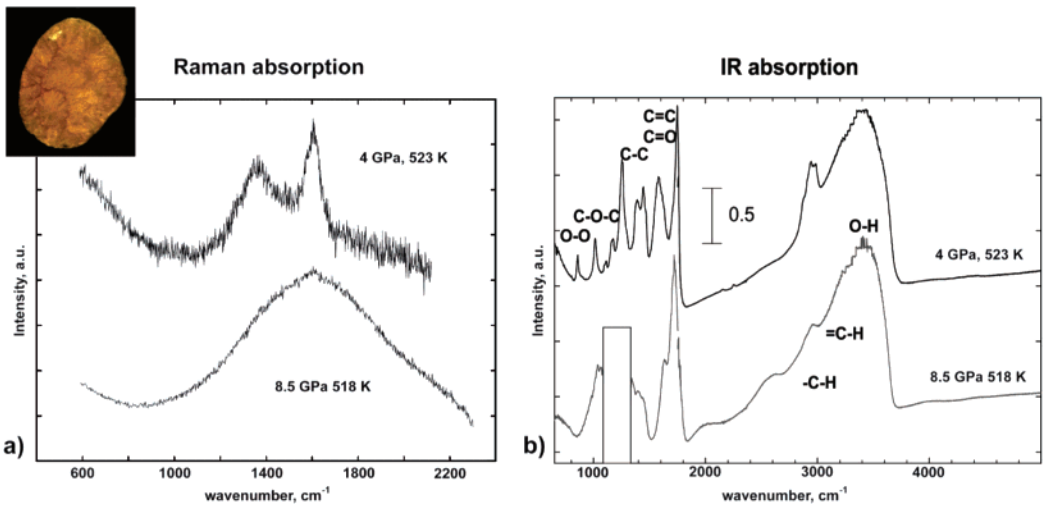

Figure 5. Raman (a) and infrared absorption (b) spectra of the C−H bend region of two different products recovered from formic acid after heating at high pressures: up to 523 K at 4 GPa (i.e., from the liquid state) and up to 518 K at 8.5 GPa (from the solid state). The spectra were collected at ambient conditions ($P = 0$ GPa and $T = 298$ K). The Raman spectra indicate the presence of microcrystalline graphite in the 4 GPa sample, with relatively sharp peaks at 1349.3 cm^{-1}(D band), 1519.7 cm^{-1} (G band), and 1591.7 cm^{-1} (D′ band).[20] The 8.5 GPa spectra less clearly indicate the presence of disordered nanocrystalline diamond, with a broad G and D′ band at 1575 cm^{-1}.[21] Complete assignments are given in Table 1. The inset is a photomicrograph of the 4.0 GPa product, which is intensely orange. These samples and results are from experiments separate from those summarized in Figure 4. Raman spectra were obtained after photoreacting the sample with a 488-nm laser.

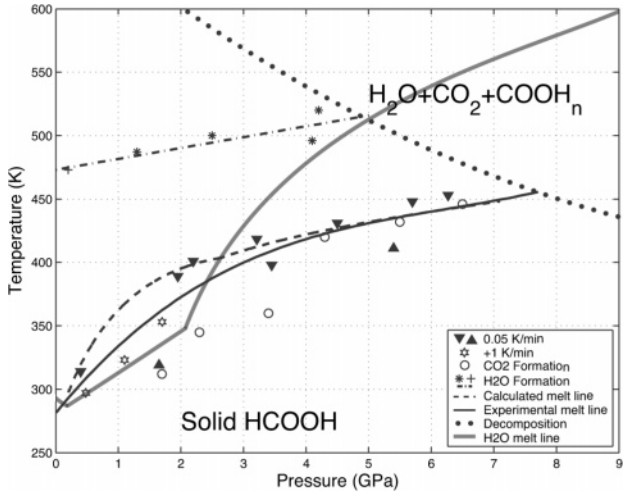

Figure 6. Experimentally determined phase and reaction diagram of formic acid, with solid and dashed lines indicating the experimental and theoretical melting curves, and the dotted lines indicating reaction boundaries. Solid triangles identify upper and lower bounds of the liquid−solid phase transition, as determined at slow heating/cooling rates of 0.05 K/min. A high-temperature chemical transformation to solid opaque products (•••) is distinguished from the decomposition of formic acid into CO_2 (and inferred H_2), which occurs near the melting line (−), and the higher-temperature decomposition of formic acid into H_2O and CO at pressures below 5 GPa (*); (+) data point taken from.[17] For comparison, the melting line for H_2O is given by the solid gray line

The spectra of the highest-pressure reaction products bear many similarities with the spectra of carbon suboxide and vinyl-ester-like polymer units obtained from carbon monoxide quenched from pressures of 5 GPa.[18] Some of the unidentified peaks, specifically those at 1390 and 1590 cm^{-1}, are consistent with the appearance of polycarbonsuboxide (C_3O_2).[19]

C. Chemical Reactions Associated with the Decomposition of Formic Acid. Figure 6 includes two curves indicating the chemical decomposition of formic acid. Three reactions have been observed in the present work: the formation of solid products discussed in Section B above, decarboxylation at approximately the temperature of melting and, below 5 GPa, dehydration at temperatures above the melting point. Figure 2 shows IR absorption spectra documenting both of these reactions: the appearance of a strong band at 2350 cm^{-1} at 398 K indicates the presence of CO_2, whereas the appearance of the bending and translational peaks of water (1620 and 600 cm^{-1}, respectively) along with a shift in the shape of the O−H band at ∼3450 cm^{-1} indicates the formation of water at 623 K.

Although we did not prove that equilibrium was fully achieved in the chemical reactions documented in our experiments, comparison with independent work does suggest a coherent picture. Specifically, both reactions have been observed in previous studies at 1 atm and elevated temperatures, and the decarboxylation reaction has been observed at pressures up to 275 bar (27.5 MPa) under hydrothermal conditions.[16] Our experiments on solid and liquid formic acid at high temperatures are consistent with these hydrothermal studies.

Discussion

Figure 6 summarizes the phase and reaction diagram of HCOOH, as determined from our high-pressure experiments. The melting curve is terminated at nearly 8 GPa by the high-temperature reactions we have documented for formic acid (Figure 5). A reaction boundary is indicated by a single line, assuming that the reactions are continuously evolving with pressure so as to be in accord with our observation that different products are quenched from different pressures. The high-temperature reactions under pressure are thus distinct from the zero-pressure decomposition, no doubt because of the strong effect of pressure on the simple-hydrocarbon reaction products in the latter case.

For comparison with our experimental results, we have calculated a melting curve for formic acid based on minimizing the two-phase (liquid−solid) Gibbs free energy of formic acid. The model combines equation-of-state and thermochemical measurements, and has been adjusted to fit available high-pressure experimental data including shock-Hugoniot measurements,[22] static-compression volumes from X-ray diffraction,[11] and impulsive light-scattering determinations of sound velocities.[23] We separate the Gibbs free energy into a reference component at one atmosphere, $G_0(T)$ describing properties at P_0 = one atmosphere, and an "equation of state" portion, $\Delta G(P)$, describing pressure effects.

$$G(P,T) = G_0(T) + \Delta G(P,T)$$

The functions $H_0(T)$ and $S_0(T)$ are expressed in terms of the constant-pressure heat capacity at one atmosphere $C_{p,0}(T)$:

$$H_0(T) = \Delta H_0 + \int_{T_0}^{T} C_{p,0}(T)\, dT \quad (1)$$

$$S_0(T) = \Delta S_0 + \int_{T_0}^{T} \frac{C_{p,0}(T)}{T}\, dT \quad (2)$$

In the present study, we take $T_0 = 298.15$ K, so ΔH_0 is the standard heat of formation and ΔS_0 is the standard entropy. We assume that the heat capacity is independent of temperature in the liquid phase and that in the solid phase it is given by a single Einstein oscillator with characteristic temperature Θ = 281 K

$$C_{p,0}(T) = 7.5R^*E(\Theta/T) \text{ where } E(x) \equiv \frac{x^2e^x}{(e^x-1)^2}$$

In the limit $T \rightarrow \infty$, C_p = 124.717 J/mole·K or 15 R. Performing the integration in eqs 1 and 2 yields

$$H_0(T) = \Delta H_0 + \theta\left[\frac{1}{e^x-1}\right]_{x_0}^{x} \quad \text{where } x \equiv \Theta/T \text{ and } x_0 \equiv \Theta/T_0 \quad (3)$$

$$S_0(T) = \Delta S_0\left[\frac{x}{e^x-1} - \ln(1-e^x)\right]_{x_0}^{x} \quad (4)$$

Given the relatively low melting temperature of formic acid to 6 GPa, we set the thermal expansion to zero, thus resulting in a simplified expression for the high-pressure Gibbs free energy component. To calculate the pressure-dependent component of the Gibbs free energy, we use the Murnaghan equation of state, which is derived by assuming a linear pressure dependence for the bulk modulus:

$$V(P) = V_0[n\kappa_0 P + 1]^{-1/n} \quad (5)$$

The pressure dependent component of the Gibbs free energy follows from $\Delta G = V\, dP - S\, dT$:

$$\Delta G(P) = \int_{P_0}^{P} V(P)\, dP \quad (6)$$

TABLE 2: Two-Phase Parameters of Formic Acid Used to Calculate the High-Pressure Melt Curve

parameter	liquid phase	solid phase
C_p (J/mol·K)	99.036	124.717
ΔH_0 (kJ/mol)	−425.100	−436.750
ΔS_0 (J/mol·K)	131.840	88.241
V_o (cc/g)	1.22	1.57
B_0 (GPa)	1.63	12.67
N	6.65	6.80

We solve for thermochemical equilibrium using concentration, temperature, and density as the independent variables. We allow for solid, liquid, and gas species in equilibrium. The variables must satisfy stoichiometric equations, balance of chemical potentials, and two thermodynamic conditions for the specified thermodynamic variables. For the case of calculating the melt curve, we use temperature and pressure as the independent variables.

The thermodynamic values that best minimize $G(P,T)$ to all available experimental data are provided in Table 2, with the heat capacity for the liquid being taken from JANAF tables, whereas that for the solid is taken from ref 22. The enthalpy and entropy for the liquid at STP are also taken from experimental data,[24,25] as is V_o.[11] The enthalpy and entropy of the solid are determined by replicating the temperature and enthalpy of melting at 1 atm pressure. The value of V_o for the solid is determined by an extrapolation of the static-compression data[11] to 1 atm. The B_o and n for the solid are fit simultaneously to the static-compression data and the initial slope of the measured melt curve. Likewise, the values of B_o and n for the liquid phase are fit to sound-speed data[23] and the initial slope of the experimental melt curve (i.e., the ratio of volume change to entropy change on fusion at one atmosphere). The relatively high error in fitting sound-speed data was due to the compromise required in order to derive the model parameters by fitting the measured slope of the melt curve.

Being limited to two phases, the model necessarily assumes congruent melting between solid and liquid, yet it is found to be in good agreement with our measurements (Figure 6). The approximations underlying our model are mitigated by our having fit experimental data in order to derive optimal parameter values (Table 2). The model was constrained to fit all available experimental data on formic acid including ambient pressure data tables. The good agreement with our measurements therefore documents how successful such a thermodynamic model can be despite its inherent simplifications.

Conclusions

Using FTIR and visual observation, we have determined the melting curve of formic acid to 8 GPa and 600 K and have characterized the decomposition reactions and chemical transformations that occur up to this pressure range. The observed melting curve is predicted reliably by a simple two-phase model that is constrained by experimental data available prior to our study. Therefore, similar models may prove useful for predicting the melting curves of other organic compounds as a function of pressure.

Because HCOOH is known to be a component of Jupiter's moons, the stability of formic acid at interior pressures and temperatures is of interest to understanding prebiotic environments in planetary science. At the base of the H_2O-dominated "oceans" or liquid mantles of Europa and Ganymede, the pressure temperature conditions are predicted to be between 0.1 and 1.5 GPa and 300−1500 K.[26,27] The frozen cores of these moons could reach pressures up to 5 GPa. It is thus possible that at the base of the ocean or in inclusions in the upper core, formic acid could chemically react to form suboxides (Figure 6). In particular, the formation of a suboxide at elevated temperatures involves the development of a more complex, polymerized structure from the simple dimer. High-pressure studies of longer organic molecules, especially those containing benzene rings, show the formation of helices and complex (double or conjugated bonds) polymers,[28] suggesting that formic acid could ultimately lead to sugars and other precursors of life.[29]

Acknowledgment. We appreciate technical assistance provided by D. W. Hansen and Phil Pagoria and continued support of our work by R. L. Simpson and L. J. Terminello. We thank C. E. Young for providing the $SrB_4O_7:Sm^{2+}$ pressure marker used in this study. W. M. is supported by a LLNL EMC fellowship. This work was performed under the auspices of the U.S. Department of Energy by the University of California, Lawrence Livermore National Laboratory under contract no. W-7405-Eng-48.

References and Notes

(1) Delsemme, A. H. *Philos. Trans. R. Soc. London, Ser. A* **1988**, *325*, 509−523.
(2) Ehrenfreund, P.; Charnley, S. B. *Annu. Rev. Astron. Astrophys.* **2000**, *38*, 427−483.
(3) Bockelee-Morvan, D.; Lis, D. C.; Wink, J. E.; Despois, D.; Crovisier, J.; Bachiller, R.; Benford, D. J.; Biver, N.; Colom, P.; Davies, J. K.; Gérard, E.; Germain, B.; Houde, M.; Mehringer, D.; Moreno, R.; Paubert, G.; Phillips, T. G.; Rauer, H. *Astron. Astrophys.* **2000**, *353*, 1101−1114.
(4) Keane, J. V.; Thielens, A. G. G.; Boogert, A. C. A.; Schutte, W. A.; Whittet, D. C. B. *Astron. Astrophys.* **2001**, *376*, 254−270.
(5) Liu, S.-Y.; Girart, J. M.; Remijan, A.; Snyder, L. E. *Astrophys. J.* **2002**, *576*, 255−263.
(6) Hollis, J. M.; Pedelty, J. A.; Snyder, L. E.; Jewell, P. R.; Lovas, F. J.; Palmer, P.; Liu, S. Y. *Astrophys. J.* **2003**, *588*, 353−359.
(7) Cazaux, S.; Thielens, A. G. G. M.; Ceccarelli, C.; Castets, A.; Wakelam, V.; Caux, E.; Parise, B.; Teyssier, D. *Astrophys. J.* **2003**, *593*, L51−L55.
(8) McCollom, T. M.; Seewald, J. S. *Geochim. Cosmochim. Acta* **2003**, *67*, 3625−3644.
(9) Shimizu, H. *Physica* **1986**, *139*, 479.
(10) Allan, D. R.; Clark, S. J. *Phys. Rev. Lett.* **1999**, *82*, 3464.
(11) Goncharov, A. F.; Manaa, M. R.; Zaug, J. M.; Gee, R. H.; Fried, L. E.; Montgomery, W. B. *Phys. Rev. Lett.* **2005**, *94*, 065505.
(12) Chervin, J. C.; Canny, B.; Besson, J. M.; Pruzan, Ph. *Rev. Sci. Instrum.* **1995**, *66*, 2595−2598.
(13) Datchi, F.; LeToullec, R.; Loubeyre, P. *J. Appl. Phys.* **1987**, *81*, 3333.
(14) Mao, H. K.; Xu, J.; Bell, P. M. *J. Geophys. Res.* **1986**, *91*, 4673.
(15) Muller, J. A.; Peytral, E. *Mem. Soc. Chem.* **1920**, 34.
(16) Maiella, P. G.; Brill, T. B. *J. Phys. Chem.* **1998**, *102*, 5886.
(17) Sharma, A.; Cody, G.; Hazen, R. M.; Hemley, R. J. *EOS Trans. Suppl.* **2000**, *81*, S52.
(18) Lipp, M.; Evans, W. J.; Garcia-Baonza, V.; Lorenzana, H. E. *J. Low Temp. Phys.* **1998**, *111*, 247.
(19) Bernard, S.; Chiarotti, G. L.; Scandolo, S.; Tosatti, E. *Phys. Rev. Lett.* **1998**, *81*, 2092.
(20) Castiglioni, C.; Mapelli, C.; Negri, F.; Zerbi, G. *J. Chem. Phys.* **2001**, *114*, 963−974.
(21) Lipp, M. J.; Baonza, V. G.; Evans, W. J.; Lorenzana, H. J. *Phys. Rev. B* **1997**, *56*, 5978−5985.
(22) Trunin, R. F.; Zhernokletoc, M. V.; Kuznetsov, N. F.; Radchenko, O. A.; Sychevskaya, N. V.; Shutov, V. V. *Khim. Fiz.* **1992**, *11*, 424.
(23) Zaug, J. M.; Howard, W. M.; Fried, L. E.; Goncharov, A. F.; Montgomery, W. B.; Crowhurst, J. C. In *Chemistry Under Extreme Conditions*, Manaa, M. R., Ed.; Elsevier Science Ltd, 2005, 399−425.
(24) Wilhoit, R. C.; Chao, J.; Hall, K. R. *J. Phys. Chem. Ref. Data* **1985**, *14*, 123.
(25) Stout, J. W.; Fisher, L. H. *J. Chem. Phys.* **1940**, *9*, 163.
(26) Sohl, F.; Spohn, T.; Breuer, D.; Nagel, K. *Icarus* **2002**, *157* 104−119.
(27) Stevenson, D. J. *Science* **2000**, *289*, 1305−1307.
(28) Katrusiak, A. *Cryst. Res. Technol.* **1991**, *26*, 523.
(29) Cooper, G.; Kimmich, N.; Belisle, W.; Sarinana, J.; Brabham, K.; Garrel, L. *Nature* **2001**, *414*, 879−883.
(30) Socrates, G. *Infrared and Raman Characteristic Group Frequencies*, 3rd ed.; Wiley: New York, 2001.